

Finite temperature and pressure molecular dynamics for BaFe₂As₂

Steffen Backes and Harald O. Jeschke

Institut für Theoretische Physik, Goethe-Universität Frankfurt, Max-von-Laue-Strasse 1, 60438 Frankfurt am Main, Germany

(Received 10 April 2013; published 5 August 2013)

We study the temperature and pressure dependence of the structural and electronic properties of the iron pnictide superconductor BaFe₂As₂. We use density functional theory-based Born-Oppenheimer molecular dynamics simulations to investigate the system at temperatures from $T = 5$ to 150 K and pressures from $P = 0$ to 30 GPa. When increasing the pressure at low temperature, we find the two transitions from an orthorhombic to a tetragonal and to a collapsed tetragonal structure that are also observed in zero temperature structure relaxations and in experiment. These transitions are considerably smeared out at finite temperature, with the critical pressure for the first transition increasing with temperature. We also analyze the electronic structure of BaFe₂As₂ at finite temperature and the effect of the structural oscillations on the band structure and Fermi surface in comparison to known zero-temperature results. Our results should be helpful for resolving some open issues in experimental reports for BaFe₂As₂ under high pressure.

DOI: [10.1103/PhysRevB.88.075111](https://doi.org/10.1103/PhysRevB.88.075111)

PACS number(s): 74.70.Xa, 71.15.Pd, 71.15.Mb, 61.50.Ks

I. INTRODUCTION

The discovery of superconductivity in FeAs-based compounds in 2008 with a critical temperature T_c up to 26 K¹ was the beginning of a large and fast-evolving field of research. These materials, such as, for example LiFeAs,^{2,3} SmFeAsO,⁴ and BaFe₂As₂⁵ share the structural motif of FeAs layers in which superconductivity can emerge either by doping and/or by external pressure with critical temperatures of up to 55 K. One material of great interest is the compound BaFe₂As₂ of the 122-type family, which shows structural phase transitions under external pressure and temperature. At room temperature and ambient pressure, the crystallographic structure of BaFe₂As₂ is that of the body-centered tetragonal ThCr₂Si₂-type structure (space group $I4/mmm$) with poor Pauli-paramagnetic metallic behavior and high electrical resistivity.⁶ Lowering the temperature, the material undergoes a structural and magnetic transition to the low-temperature orthorhombic $Fmmm$ structure,⁷ with a stripe-ordering of the Fe magnetic moments.⁸ External hydrostatic or uniaxial pressure is capable of suppressing the magnetically ordered orthorhombic phase and induces a tetragonal paramagnetic phase with a region of superconductivity^{9–11} at low temperatures. At higher pressures, the collapsed tetragonal phase emerges,^{12,13} where experiments as well as recent theoretical investigations¹⁴ find different values for the critical pressure, which seems to be sensitive to temperature. At 300 K, values of 16.7 GPa under nonhydrostatic pressure conditions¹² and 27 GPa¹³ under hydrostatic pressure conditions are reported, whereas at 33 K a critical pressure of 29 GPa was found.¹³ Also, hysteresis effects of the temperature or a coexistence of the orthorhombic and tetragonal phase might be present for a wide range of pressures.¹³ These experimental results show that the critical pressures and their possible temperature dependence are not yet fully understood.

In recent years, there have been quite a few theoretical studies of structural effects in BaFe₂As₂. The phase transitions at zero temperature were studied with Car Parrinello molecular dynamics with friction,¹⁵ highlighting the importance of Fermi surface nesting for the nature of the phase transitions.

A combination of DFT total energies and thermodynamical quantities estimated from experiment was used to rationalize some finite temperature transition points in the phase diagram.¹⁶ Constant volume DFT relaxations have been used to study the zero temperature pressure-induced structural transitions and equation of state both for hydrostatic¹⁷ and nonhydrostatic¹⁸ pressure conditions. The phase transitions in BaFe₂As₂ have also been studied using the fast inertial relaxation engine,¹⁴ which allows an unconstrained equilibrium structure search for arbitrary stress tensors. This method has been used to work out effects of uniaxial pressure along c direction¹⁴ and also in the ab plane.¹⁹ The phase transitions from a paramagnetic tetragonal phase to an orthorhombic phase with spin density wave order via a nematic phase have been studied based on the Heisenberg model.^{20,21} A detailed study in terms of a Ginzburg-Landau effective action can be found in Ref. 22. Note that these investigations address structural effects caused by quantum fluctuations that are beyond the scope of the present study.

Since most studies so far used either experimentally measured or zero-temperature optimized structures, the complex temperature and pressure phase diagram of BaFe₂As₂ calls for microscopic first principles calculations at finite temperature. We study BaFe₂As₂ at finite temperatures and pressures by employing *ab initio* density functional theory (DFT) methods combined with finite temperature and pressure molecular dynamics. As is well known, straightforward density functional theory doesn't take into account the disordered local moments that would be necessary for describing the ambient pressure paramagnetic phase at high temperature. Therefore, in this study we focus on how the zero temperature structural phase transitions under pressure extend to finite temperatures and determine the electronic properties of the various phases at finite temperature. By shedding some light on the finite temperature regime with external pressure, we think our study can provide a useful complement to existing $T = 0$ K theoretical calculations and can help to clarify the contradicting observations that are reported for the transition pressures in experiments.

II. METHODS

We performed molecular dynamics calculations using the atomic simulation environment (ASE)²³ interface combined with the DFT Vienna *ab initio* simulation package (VASP),²⁴ version 5.2.11, with the projector augmented wave basis²⁵ in the generalized gradient approximation (GGA) by Perdew, Burke, and Ernzerhof.²⁶ To control the temperature and pressure, the Berendsen dynamics²⁷ provided by ASE were employed, using characteristic time constants of $\tau_T = 50$ fs and $\tau_P = 250$ fs for the thermostat and barostat, respectively, and a time step of 1 fs for the integration of the equations of motion. The energy cut-off in VASP was set to 400 eV and a Monkhorst-Pack uniform grid of $(4 \times 4 \times 4)$ k points was used for the integration of the Brillouin zone. To account for the magnetic stripe order, we simulate a $\sqrt{2} \times \sqrt{2} \times 1$ supercell of the conventional orthorhombic unit cell of BaFe_2As_2 containing 8 Fe atoms. Calculations were performed on a pressure-temperature grid with 13 different values of P going from 0 to 30 GPa in 2.5 GPa steps and for temperatures of 5, 50, 100, and 150 K. The values of observables were obtained by averaging over the last 400 fs of the trajectory after the configuration was sufficiently equilibrated.

III. RESULTS

A. Temperature effect on pressure-induced phase transitions

We now present our results for the lattice parameters, magnetic moments, and volume at temperatures between 5 and 150 K compared to a zero-temperature relaxation.¹⁴ In Fig. 1 we show the pressure dependence of the three lattice parameters a , b , and c at $T = 5$ K, which is very similar to the $T = 0$ K case. We observe a transition from the orthorhombic to tetragonal structure at about 12.5 GPa and a second transition from the tetragonal to a collapsed tetragonal structure which is around 25 GPa. For low values of pressure, i.e., 0–5 GPa, our results are almost identical to the $T = 0$ K

calculation, with our obtained values for the a and b axis being slightly longer in comparison. The reason for that is clearly given by finite temperature, which leads to internal pressure due to vibrating atomic positions and, thus, increasing the volume of the unit cell compared to the $T = 0$ K case.

The position of the transition to the tetragonal phase is visible as a sudden increase in the lattice parameter b at around 12.5 GPa. The position of the transition is in agreement with the $T = 0$ K result, but the resulting configuration is not a perfect tetragonal unit cell, with the orthorhombic distortion significantly reduced but still nonzero. The $\frac{a}{b}$ ratio drops from 1.013 at 10 GPa to 1.009 at 12.5 GPa and retains a value larger than one up to 17.5 GPa.

Even though all the lattice parameters noticeably differ from the $T = 0$ K results in some cases, our obtained volume of the unit cell is still very similar [see Fig. 1(c)].

For increasing pressure, we find the average distance of the iron and arsenic atoms in the Fe-As tetrahedron layers to be reduced and the orthorhombic transition is visible as a kink in the Fe-As distance plot. Our results closely match the zero-temperature calculation and correctly indicate the orthorhombic to tetragonal transition around 12.5 GPa [see Fig. 1(f)].

The tetragonal to collapsed tetragonal transition at zero temperature is marked by a sudden increase of the a and b and a decrease in the c lattice constant at 27.5–30 GPa. Our results show a smoothed-out transition with less drastic changes in the lattice parameters at $P = 22.5$ –25 GPa. The a and b lattice parameters increase by 0.23% from 22.5 to 25 GPa, whereas the increase for $T = 0$ K is 0.66% from 27 to 30 GPa. The c lattice parameter shows a similar behavior, whereas in the zero-temperature case a distinct decrease at 27.5–30 GPa is visible, but our results show a smooth behavior of c that looks almost linear with no sharp drop.

The most notable difference between finite-temperature and previous zero-temperature results is the nontetragonal but intermediate orthorhombic-tetragonal structure of our system for values of pressure where the $T = 0$ K structure is already

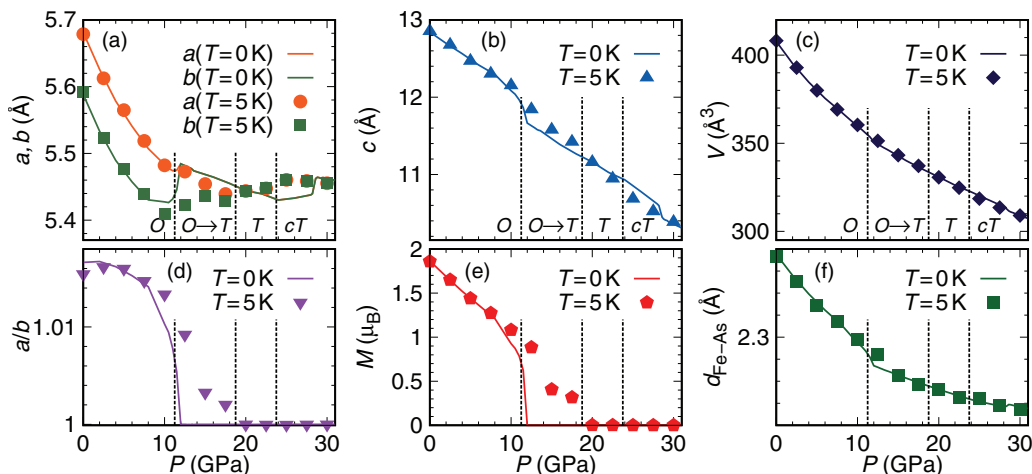


FIG. 1. (Color online) Structural parameters for BaFe_2As_2 at $T = 5$ K as a function of pressure (symbols). (a) Time averaged a and b lattice parameters, where a is in the direction along the AFM ordering of the magnetic moments. (b) Time averaged c lattice parameter. (c) Volume of the unit cell comprising 8 Fe atoms. (d) a/b ratio, (e) absolute value of the (time and unit cell averaged) Fe magnetic moment, and (f) the Fe-As distance, averaged over time and all nearest-neighbor Fe-As bonds. The solid line is a $T = 0$ K optimized structure from Ref. 14.

completely tetragonal. Thus, our calculations obtain a smooth transition rather than sudden change of the lattice parameters for the $O \rightarrow T$ transition and also for the $T \rightarrow cT$ transition. This is to be expected since due to the finite temperature the system is allowed to oscillate between two competing structural configurations and magnetic orderings close to the critical pressure at $T = 0$ K. Our result suggests that this phase, which is intermediate between orthorhombic and tetragonal phases, is the best approximation we can get with our 20 atom supercell to a mixed phase. As a result, the $O \rightarrow T$ transition is smoothed out to higher pressures, whereas the $T \rightarrow cT$ transition experiences strong smearing effects. This behavior is strongly enhanced for higher temperature, whereas the $O \rightarrow T$ transition is shifted to even higher pressures of about 15 GPa and the $T \rightarrow cT$ transition becomes almost indiscernible. This gives interesting effects in the relative change of the lattice parameters with temperature, which we will discuss below.

The increase of the volume of the unit cell and the lattice parameters a , b , and c with temperature can be seen in Fig. 2. For 50 K the volume increases slightly at all pressures compared to $T = 5$ K, with different behavior at the critical

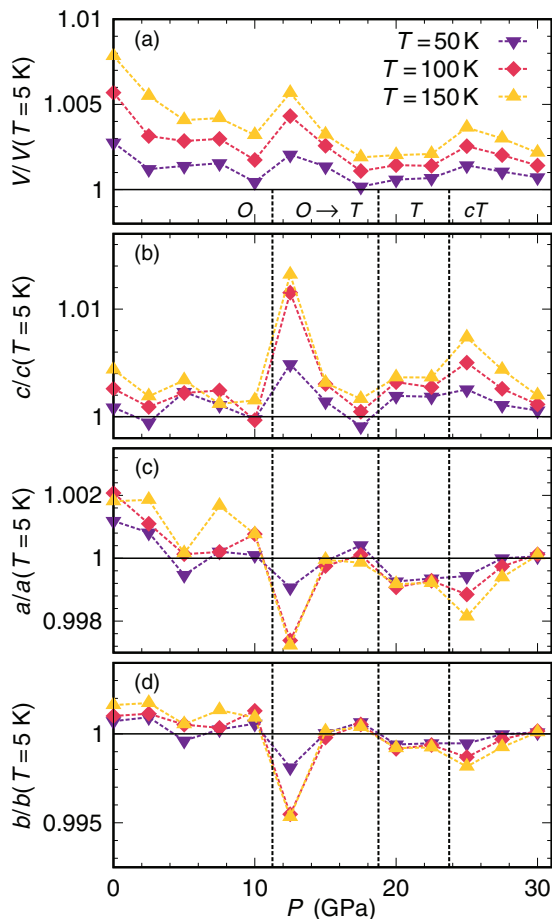


FIG. 2. (Color online) The relative increase of the volume V of the unit cell and the lattice parameters a , b , and c compared to $T = 5$ K at different temperatures as a function of external pressure. The dashed vertical lines indicate the critical pressure that we identified for the corresponding structural transitions at $T = 5$ K. Note that in particular the first phase transition shifts to higher pressures as the temperature is increased.

pressures. Up to the first transition, the increase of the volume with temperature decreases as expected due to higher pressure and then shows a peak right at 12.5 GPa, which is caused by the temperature-induced shift of the $O \rightarrow T$ transition, i.e., the sudden decrease in volume, to higher pressures. In all of the regions we identified, except in the tetragonal phase, the relative volume increase falls off almost monotonically until the transition to the next phase, where it shows a small jump to higher values, after which it decreases again. Only in the tetragonal phase the increase with temperature seems to be pressure-independent. Comparatively, the jump of the relative volume increase is largest at the high pressure end of the orthorhombic phase. This behavior is mirrored in the temperature dependence of the c lattice parameter at the critical pressures. We observe that at a pressure of $P = 12.5$ GPa, the relative change of c when increasing the temperature from $T = 5$ to 50 K and from $T = 50$ to 100 K compared to $T = 100$ to 150 K is considerably larger. This can be explained by the temperature-induced transition from the tetragonal phase to the orthorhombic phase. This is also the reason for the relative decrease of the a and b lattice parameters at 12.5 GPa. Thus, we obtain a positive slope of the orthorhombic to tetragonal phase transition in the temperature-pressure phase diagram of BaFe_2As_2 .

Finally, we set up a temperature pressure phase diagram by specifying the state of the system for each (T, P) combination we calculated, i.e., by taking into account if the structure is orthorhombic or tetragonal, the magnetic moments, etc. To determine the transition pressures used in the diagram we investigated the pressure derivative of the a , b , and c lattice parameters and the volume. In the phase diagram (see Fig. 3), we distinguished four different regions of structural configurations: The first one is the phase of the purely orthorhombically distorted unit cell, in which all the lattice parameters still continue to decrease monotonically with higher pressure. As we have seen, this phase is present for pressures up to $P = 10$ GPa for the temperatures $T = 5$ and 50 K and extends to $P = 12.5$ K for the two higher temperatures. The second region is an intermediate orthorhombic-tetragonal state, in which the shorter axis b of the unit cell is no longer decreasing

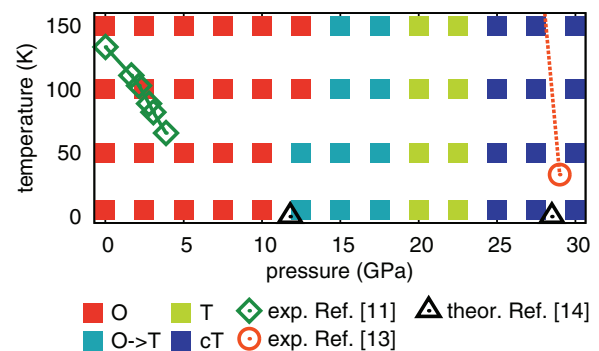


FIG. 3. (Color online) The temperature-pressure phase diagram of BaFe_2As_2 , where we distinguish between four different phases (see detailed explanation in the text). Experimental data points by Colombier *et al.*¹¹ (green line) represent the $O \rightarrow T$ transition and the data by Mittal *et al.*¹³ (orange symbols) represents the $T \rightarrow cT$ transition. The two black data points obtained by a $T = 0$ K relaxation by Tomić *et al.*¹⁴ also indicate the two critical pressures.

but increases with higher pressures and has not reached the same length as the longer axis a . This region is quite prominent in our results since the transition is always smoothed out considerably compared to the $T = 0$ K result.¹⁴ The next phase is the one of a pure tetragonal unit cell with equal lattice parameters $a = b$. After that, at high pressures the collapsed tetragonal phase is dominating, which is defined by the sudden increase in the a and b and the decrease in the c axis. By comparing the temperature-dependence of the lattice parameters at fixed values of the pressure, we suspect the $T \rightarrow cT$ transition to be pushed to lower pressures at higher temperature, which was found by Mittal *et al.*,¹³ but due to strong smearing effects we could not determine a slope in the critical pressure. However, in general we already observe the transition to the collapsed tetragonal phase at a pressure being 5–7.5 GPa lower compared to experiments.

B. Finite temperature and pressure band structure

In order to investigate the effect of the vibrational structural deformations on the electronic properties of BaFe_2As_2 at finite temperature, we performed band structure calculations using the full-potential local-orbital minimum-basis code (FPLO).²⁸ For the calculation, a $6 \times 6 \times 6$ \mathbf{k} mesh was employed and the generalized gradient approximation (GGA) method by

Perdew, Burke, and Ernzerhof²⁶ was used for the exchange and correlation potential. The tetrahedron-integration method was used for the integration of the Brillouin zone, and the density was converged with an accuracy of 10^{-6} .

As the first configuration, we investigated a temperature of $T = 100$ K and pressure of $P = 0$ GPa, where an orthorhombic unit cell with nonzero magnetic moments is present. At this temperature, the volume is periodically oscillating around a mean value of $410.747 \text{ \AA}^3 \pm 0.07\%$. The duration for a complete vibrational cycle of the volume is about 210 fs. We took snapshots of the crystal structure in 10-fs intervals, starting from the maximal expanded volume down to the minimum value of the volume, so in total we covered one half of the oscillation cycle of about 100 fs. For the band structure, we use the usual path in \mathbf{k} -space $\Gamma = (0,0,0)$, $X = (1/2,0,0)$, $M = (1/2,1/2,0)$, Γ , $Z = (0,0,1/2)$, given in units of the reciprocal lattice vectors. We chose this path since it corresponds to the higher symmetry of the Fe lattice rather than to the $Fmmm$ space group and it can be easily compared to the band structure of the more simple tetragonal LaOFeAs .²⁹

We compared our results to a zero-temperature BaFe_2As_2 structure at $P = 0$ GPa from Ref. 14 to investigate how the finite temperature affects the bands near the Fermi level. Since the most important contribution to the DOS at the Fermi level in this materials is usually given by the Fe bands, which we

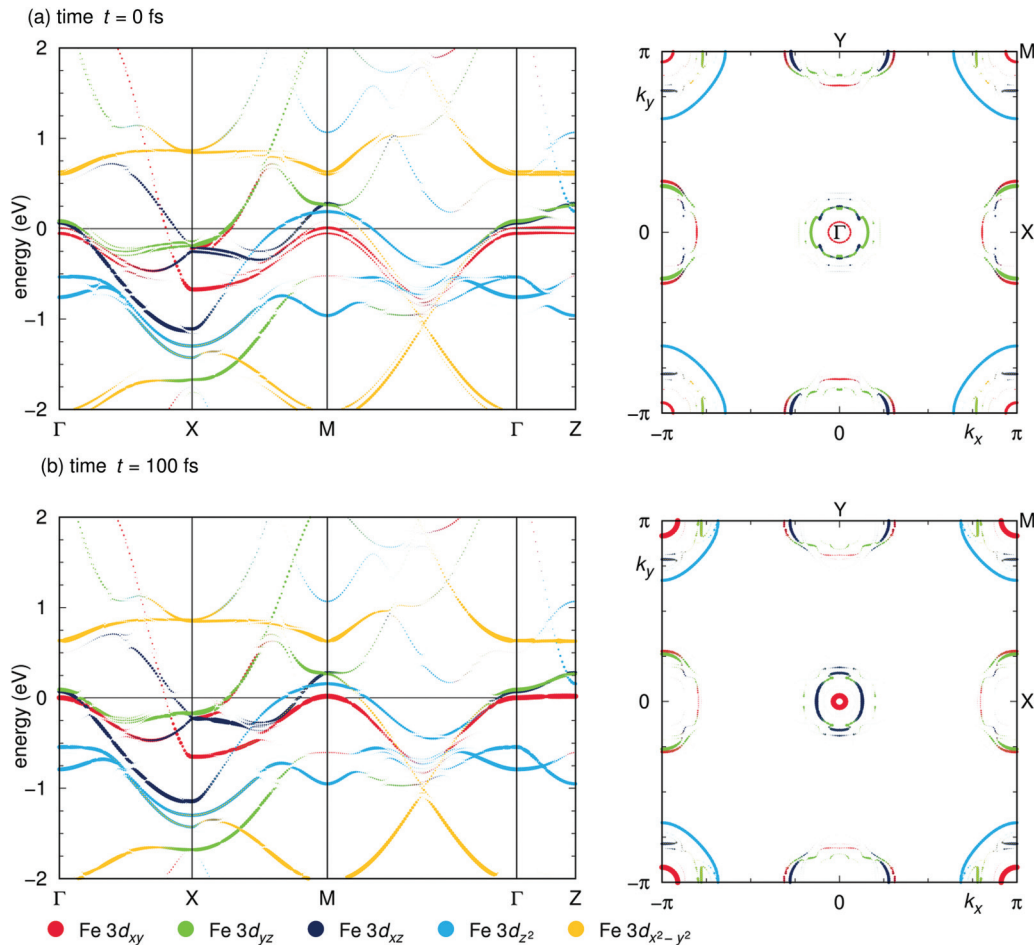


FIG. 4. (Color online) Band structure of BaFe_2As_2 and $k_z = 0$ Fermi surface cut at $T = 100$ K and different times within one MD trajectory.

also confirmed to be the case here, we will now discuss the effect of the finite temperature on the Fe bands exclusively. For a meaningful comparison, one has to keep in mind that in the finite-temperature case the positions of the atoms in the unit cell are varying in time and, thus, the eight Fe atoms are no longer equivalent and the crystal structure is no longer the $Fm\bar{3}m$ space group but rather triclinic $P1$. Due to the higher number of inequivalent Fe atoms we also get additional

Fe bands that are folded back into the Brillouin zone. By using the unfolding method that was proposed in Ref. 30 and implemented in FPLO,³¹ we can unfold the band structure and map the equivalent bands onto a single one.

In Fig. 4, we show the Fe orbital weighted band structure and the $k_z = 0$ Fermi surface cut of BaFe_2As_2 at $T = 100$ K and ambient pressure. The figure shows instantaneous electronic structures for two structural configurations during

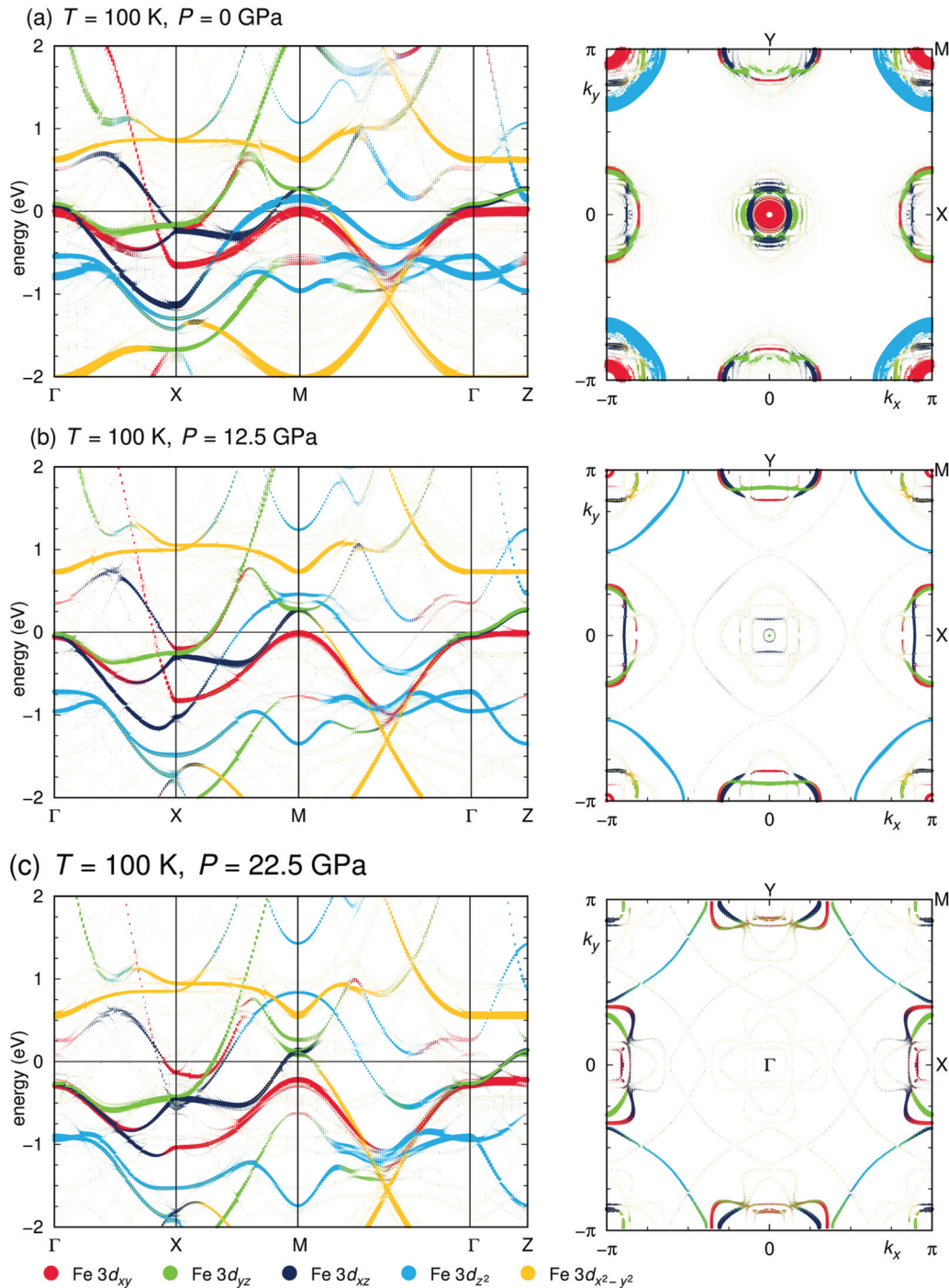


FIG. 5. (Color online) Time-averaged band structures and $k_z = 0$ Fermi surface cuts at a temperature $T = 100$ K for three different pressures. (a) $P = 0$ GPa corresponds to the orthorhombic phase, (b) $P = 12.5$ GPa is in the intermediate region between orthorhombic and tetragonal phases, and (c) $P = 22.5$ GPa corresponds to the tetragonal phase. Averaging over several electronic structures along an MD trajectory leads to significant broadening of bands and Fermi surface contours, especially at low pressure.

a complete volume oscillation cycle of the unit cell, separated by a time of $t = 100$ fs. The first configuration [Fig. 4(a)] corresponds to the maximal volume and the second one [Fig. 4(b)] to the minimal volume during the oscillation cycle. Close to the Fermi level E_F , the most important bands are the Fe $3d_{xy}$, $3d_{xz}$, and $3d_{yz}$ states. The unfolding procedure occasionally leads to more crossings of the Fermi surface than at $T = 0$ because in their thermal motion the Fe sites are only approximately equivalent. Fe $3d_{xy}$, $3d_{xz}$, and $3d_{yz}$ bands form hole pockets at the Γ point and in addition $3d_{z^2}$ character is present at the M point. Electron pockets at the X (and Y) points are of $3d_{xy}$, $3d_{xz}$, and $3d_{yz}$ character. Compared to $T = 0$ K calculations, the effect of the finite temperature is clearly present in the shallow inner hole pocket of $3d_{xy}$ character at the Γ point, which clearly shows oscillations in its size during the trajectory. Shrinking of this hole pocket can be compared to the effect of hydrostatic and uniaxial pressure,¹⁴ where the Fe $3d_{xy}$ band is pushed below the Fermi level at the magnetic $O \rightarrow T$ transition. The structural variations along the MD trajectory at $T = 100$ K also show interesting effects on the outer hole cylinders at the Γ point. While they appear elliptical along k_y at $t = 0$ fs, they appear elliptical along k_x at $t = 100$ fs. This change of shape goes hand in hand with changing importance of $3d_{yz}$ and $3d_{xz}$ characters: more $3d_{yz}$ at $t = 0$ fs, more $3d_{xz}$ at $t = 100$ fs. This feature resembles the electronic structure changes upon uniaxial compressive and tensile stress in the ab plane of BaFe_2As_2 (compare Ref. 19). Other bands seem to be less affected by the vibrational excitation.

We now proceed from the consideration of transient shapes of the Fermi surface to its thermal average. Transient features of the electronic structure are interesting theoretically and can in principle, at least following the excitation of coherent phonons, be observed in experiments with very high temporal resolution.^{32,33} Since usual angle resolved photo emission observes time-averaged electronic structures, a comparison to the averaged band structures like the ones we show in Fig. 5 might be more appropriate. Note, however, that while our electronic structures include the effect of thermally vibrating crystal structures, they do not include the thermal broadening of the spectral function, which can be described

by finite temperature Greens functions. Figure 5 shows the time-averaged band structure at $T = 100$ K for the pressures $P = 0, 12.5,$ and 22.5 GPa, where the first one is deep in the orthorhombic phase, the second is in the smooth transition region between orthorhombic and tetragonal phases, and the latter is in the tetragonal phase.

Our results clearly show that the Fe $3d_{z^2}$ band at the M point and the Fe $3d_{xy}$ band at the Γ and M points experience noticeable changes due to the excitation of phonons at finite temperature. In the plot, the broadening of the bands is a lot larger than the line width used to draw them, which has implications for interpreting and comparing theoretical iron pnictide band structures and experimentally measured spectral functions. Bands that are below the Fermi level in theoretical zero-temperature calculations can become partially occupied even at temperatures way below room temperature, like $T = 100$ K, just because of the thermal vibrations. This could have implications for the interpretation of angle-resolved photo emission spectroscopy (ARPES) results as it leads to an additional broadening in spectral functions, besides the usual thermal broadening. In fact, our thermally averaged band structures and Fermi surfaces can be seen as a microscopic analog to the estimate of thermal effects in ARPES using Debye-Waller factors.³⁴

As the pressure is increased to 12.5 GPa, which in our case is in the orthorhombic-tetragonal smoothed transition region, we notice a significant shift of bands away from the Fermi level as already reported previously.^{14,15} The Fe $3d_{xy}$ band becomes fully occupied at the Γ point and oscillates around E_F at the M point, whereas the Fe $3d_{z^2}$ band is shifted to higher energies. The finite Fe $3d_{xy}$ weight at the Fermi level at the M point is in contrast to the previous $T = 0$ K calculation¹⁴ and corresponds to the smooth $O \rightarrow T$ transition. Compared to the $P = 0$ GPa result, the temperature-induced oscillations are greatly reduced and only little smearing of the Fermi surface is observed.

In the tetragonal phase at 22.5 GPa the Fe bands are pushed further away from the Fermi level, with no crossings at the Γ point and only small Fe $3d_{yz}$ and $3d_{xz}$ hole pockets at the M point. Thermal smearing of the Fermi surface is further reduced.

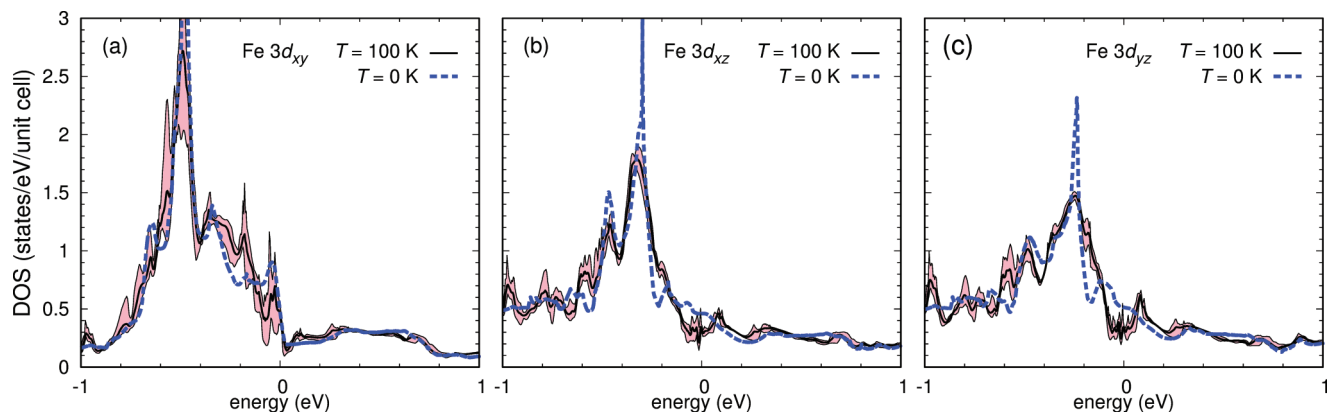


FIG. 6. (Color online) Partial densities of states, compared at $T = 0$ K (dashed line)¹⁴ and $T = 100$ K (solid line) for the three Fe t_{2g} orbitals $3d_{xy}$, $3d_{xz}$, and $3d_{yz}$. The solid line is the averaged DOS and the colored area indicates the extent of the variation due to temperature (see detailed explanation in the text).

The effect of the structural oscillation in the Fe bands is also visible in the density of states (DOS). In Fig. 6 we show the Fe 3d density of states for the three most important Fe $3d_{xy}$, $3d_{yz}$, and $3d_{xz}$ bands. Compared to the zero-temperature case, we find our previous results for the $T = 100$ K calculations to be confirmed also in the DOS. The change of the DOS for energies above E_F is rather subtle, while below we see a general shift of weight to lower energies or an increase of the DOS compared to $T = 0$ K. Right at the Fermi level and slightly below the change is strongest, where the DOS is significantly reduced. This lowering of the density of states at the Fermi level $N(E_F)$ is due to a lowering of the symmetry of the system at finite temperature, which reduces the energetically unfavorable large $N(E_F)$ (Stoner instability). The effect of the temperature-induced oscillating structural configuration is clearly visible with an average variation of the DOS of about $\sim 15\text{--}20\%$ around the mean value below the Fermi level and $\sim 5\text{--}10\%$ above. Right at E_F this effect seems to reach a local maximum and can approach large peak values of about $\sim 40\%$, like in the Fe $3d_{xy}$ orbital at -0.05 eV. For higher pressures we find the variations in the DOS to be reduced as expected and do not show them here.

IV. CONCLUSIONS

We used density functional theory-based Born-Oppenheimer molecular dynamics to study the behavior of BaFe_2As_2 under external pressure and finite temperature. For low temperatures, our results are in agreement with existing experimental as well as other theoretical results, correctly indicating the transition from the orthorhombic magnetic structure to a tetragonal paramagnetic phase around 12.5 GPa and the tetragonal to a collapsed tetragonal phase around ~ 25 GPa. In general, the transitions were found to

be considerably smoothed out due to finite temperature and the critical pressure for the O \rightarrow T transition was shifted to higher pressures, whereas the T \rightarrow cT transition becomes almost indiscernible. These effects became more enhanced with higher temperature and we found a positive slope of the O \rightarrow T transition line in the temperature-pressure phase diagram. Thus, our results confirm that temperature is an important factor for the structural transitions in BaFe_2As_2 .

We also investigated the electronic structure of BaFe_2As_2 and the effect of structural oscillations at finite temperature on the band structure and density of states. At $T = 100$ K and $P = 0$ GPa, we find the size of the hole pockets at the Γ and M symmetry points to be oscillating significantly in time. The Fe $3d_{xy}$ band shows strong oscillations at E_F with significant variations in the DOS, and Fe $3d_{xz}$ and $3d_{yz}$ weights are periodically oscillating at the Γ point due to the temperature-induced periodic changes in the structural configuration. At ambient pressure, the oscillations in the band energies caused by temperature are significant and lead to a thermal broadening of the Fermi surface. Therefore, compared to zero-temperature calculations, which miss the dynamical oscillations and overestimate the DOS at the Fermi level, our results indicate that these effects cause nonnegligible changes in the electronic structure even at temperatures well below room temperature, which could be important for the interpretation of experiments like angle-resolved photo emission spectroscopy.

ACKNOWLEDGMENTS

The authors thank Roser Valentí for useful discussions and gratefully acknowledge financial support by the Deutsche Forschungsgemeinschaft through Grant No. SPP 1458. We thank the Centre for Scientific Computing (CSC, LOEWE-CSC) in Frankfurt for computing facilities.

¹Y. Kamihara, T. Watanabe, M. Hirano, and H. Hosono, *J. Am. Chem. Soc.* **130**, 3296 (2008).

²J. H. Tapp, Z. Tang, B. Lv, K. Sasmal, B. Lorenz, P. C. W. Chu, and A. M. Guloy, *Phys. Rev. B* **78**, 060505(R) (2008).

³X. C. Wang, Q. Q. Liu, Y. X. Lv, W. B. Gao, L. X. Yang, R. C. Yu, F. Y. Li, and C. Q. Jin, *Solid State Commun.* **148**, 538 (2008).

⁴Z.-A. Ren, G.-C. Che, X.-L. Dong, J. Yang, W. Lu, W. Yi, X.-L. Shen, Z.-C. Li, L.-L. Sun, F. Zhou, and Z.-X. Zhao, *Europhys. Lett.* **83**, 17002 (2008).

⁵M. Rotter, M. Tegel, and D. Johrendt, *Phys. Rev. Lett.* **101**, 107006 (2008).

⁶X. F. Wang, T. Wu, G. Wu, H. Chen, Y. L. Xie, J. J. Ying, Y. J. Yan, R. H. Liu, and X. H. Chen, *Phys. Rev. Lett.* **102**, 117005 (2009).

⁷M. Rotter, M. Tegel, D. Johrendt, I. Schellenberg, W. Hermes, and R. Pöttgen, *Phys. Rev. B* **78**, 020503(R) (2008).

⁸Q. Huang, Y. Qiu, W. Bao, M. A. Green, J. W. Lynn, Y. C. Gasparovic, T. Wu, G. Wu, and X. H. Chen, *Phys. Rev. Lett.* **101**, 257003 (2008).

⁹P. L. Alireza, Y. T. Chris Ko, J. Gillett, C. M. Petrone, J. M. Cole, G. G. Lonzarich, and S. E. Sebastian, *J. Phys.: Condens. Matter* **21**, 012208 (2008).

¹⁰J. Paglione and R. L. Greene, *Nature Phys.* **6**, 645 (2010).

¹¹E. Colombier, S. L. Budko, N. Ni, and P. C. Canfield, *Phys. Rev. B* **79**, 224518 (2009).

¹²W. Uhoja, A. Stemshorn, G. Tsoi, Y. K. Vohra, A. S. Sefat, B. C. Sales, K. M. Hope, and S. T. Weir, *Phys. Rev. B* **82**, 144118 (2010).

¹³R. Mittal, S. K. Mishra, S. L. Chaplot, S. V. Ovsyannikov, E. Greenberg, D. M. Trots, L. Dubrovinsky, Y. Su, Th. Brueckel, S. Matsuishi, H. Hosono, and G. Garbarino, *Phys. Rev. B* **83**, 054503 (2011).

¹⁴M. Tomić, R. Valentí, and H. O. Jeschke, *Phys. Rev. B* **85**, 094105 (2012).

¹⁵Y. Z. Zhang, H. C. Kandpal, I. Opahle, H. O. Jeschke, and R. Valentí, *Phys. Rev. B* **80**, 094530 (2009).

¹⁶W. Ji, X. W. Yan, and Z. Y. Lu, *Phys. Rev. B* **83**, 132504 (2011).

¹⁷N. Colonna, G. Profeta, A. Continenza, and S. Massidda, *Phys. Rev. B* **83**, 094529 (2011).

- ¹⁸N. Colonna, G. Profeta, and A. Continenza, *Phys. Rev. B* **83**, 224526 (2011).
- ¹⁹M. Tomić, H. O. Jeschke, R. M. Fernandes, and R. Valentí, *Phys. Rev. B* **87**, 174503 (2013).
- ²⁰C. Fang, H. Yao, W.-F. Tsai, J. P. Hu, and S. A. Kivelson, *Phys. Rev. B* **77**, 224509 (2008).
- ²¹C. Xu, M. Müller, and S. Sachdev, *Phys. Rev. B* **78**, 020501(R) (2008).
- ²²R. M. Fernandes, A. V. Chubukov, J. Knolle, I. Eremin, and J. Schmalian, *Phys. Rev. B* **85**, 024534 (2012).
- ²³S. R. Bahn and K. W. Jacobsen, *Comput. Sci. Eng.* **4**, 56 (2002).
- ²⁴G. Kresse and J. Hafner, *Phys. Rev. B* **47**, 558 (1993); **49**, 14251 (1994); G. Kresse and J. Furthmüller, *Comput. Mat. Sci.* **6**, 15 (1996); *Phys. Rev. B* **54**, 11169 (1996).
- ²⁵P. E. Blöchl, *Phys. Rev. B* **50**, 17953 (1994); G. Kresse and D. Joubert, *ibid.* **59**, 1758 (1999).
- ²⁶J. P. Perdew, K. Burke, and M. Ernzerhof, *Phys. Rev. Lett.* **77**, 3865 (1996); **78**, 1396 (1997).
- ²⁷H. Berendsen, J. Postma, W. van Gunsteren, A. DiNola, and J. R. Haak, *J. Chem. Phys.* **81**, 3684 (1984).
- ²⁸K. Koepnik and H. Eschrig, *Phys. Rev. B* **59**, 1743 (1999); <http://www.FPLO.de>
- ²⁹I. I. Mazin, D. J. Singh, M. D. Johannes, and M. H. Du, *Phys. Rev. Lett.* **101**, 057003 (2008).
- ³⁰W. Ku, T. Berlijn, and C.-C. Lee, *Phys. Rev. Lett.* **104**, 216401 (2010).
- ³¹E. van Heumen, J. Vuorinen, K. Koepnik, F. Massee, Y. Huang, M. Shi, J. Klei, J. Goedkoop, M. Lindroos, J. van den Brink, and M. S. Golden, *Phys. Rev. Lett.* **106**, 027002 (2011).
- ³²L. Rettig, R. Cortés, S. Thirupathaiah, P. Gegenwart, H. S. Jeevan, M. Wolf, J. Fink, and U. Bovensiepen, *Phys. Rev. Lett.* **108**, 097002 (2012).
- ³³I. Avigo, R. Cortés, L. Rettig, S. Thirupathaiah, H. S. Jeevan, P. Gegenwart, T. Wolf, M. Ligges, M. Wolf, J. Fink, and U. Bovensiepen, *J. Phys.: Condens. Matter* **25**, 094003 (2013).
- ³⁴L. Plucinski, J. Minár, B. C. Sell, J. Braun, H. Ebert, C. M. Schneider, and C. S. Fadley, *Phys. Rev. B* **78**, 035108 (2008).